IET Generation, Transmission & Distribution

Special Issue on Power Electronic Converter Systems for Integration of Renewable Energy Sources

IET Journals
The Institution of Engineering and Technology

Real time implementation of artificial neural networks-based controller for battery storage supported wind electric generation

ISSN 1751-8687
Received on 30th May 2014
Revised on 4th November 2014
Accepted on 6th January 2015
doi: 10.1049/iet-gtd.2014.0544
www.ietdl.org

Sony Kurian ✉, *Sindhu T. Krishnan*, *Elizabeth P. Cheriyan*

Department of Electrical Engineering, National Institute of Technology, Calicut, India
✉ *E-mail: sonykurian@rediffmail.com*

Abstract: Energy storage systems have established their capability to overcome the problems caused by intermittent nature of renewable sources when integrated to existing grid. Voltage and frequency control, as well as load shifting can be done using grid level storage systems incorporated with renewable sources. They can effectively serve the system as an energy sink and source. Operational use of energy storage for grid level support of a wind electric generator (WEG) is demonstrated in this study. The battery storage supported WEG along with controllers is modelled. Artificial neural network controller, which is having inherent learning capability, is developed to regulate the power flow between wind generator and utility grid. The proposed algorithm and the corresponding controller are simulated in MATLAB/Simulink and implemented in the DSP processor. The real time data exchange between Simulink and the floating point DSP processor TMSF32028335 is realised using on-board JTAG emulator. The hardware implementation using DSP processor presented in this work establishes the efficacy of the proposed control strategy for real time applications.

1 Introduction

The addition of carbon free renewable electricity generation technologies has created a number of regulatory and performance issues in the utility grid worldwide. These issues are the outcome of extremely intermittent nature of these renewable resources. Once the penetration level of these resources increases, isolated grids and insufficient transmission infrastructure make the situation much more critical [1]. Modern variable-speed wind turbines and large photovoltaic power plants connected to the utility grid do not contribute to the frequency stability as the synchronous generators of the conventional gas or steam turbine do [2]. Within the fragmented and deregulated energy market, it is very essential for the independent power producers to follow the policies and amendments put forward by the utility so as to maintain the grid codes throughout the integrated operation. Grid level storage can serve the system as an energy sink and source [3]. They can store energy during unfavourable market conditions and during low load hours. The stored energy can be dispatched to meet the load requirement during the time of low generation. The reliability and availability of the system can be increased to a greater extent by the utilisation of energy storage devices alongside the renewable sources [4]. Grid level storage systems can also provide decoupling between the generation and the load ensuring the intermittent nature of renewable sources not affecting the quality of power in the grid by smoothing power output [5, 6], and effectively help in damping inter area oscillations [7].

As of now, more than 90% of the total electricity storage is provided by pumped hydroelectric storage (PHS) [8]. This is the most prominent and well-established storage technology. Environmental and geographical limitations restrict new pumped hydro installations. Compressed air energy storage (CAES) dominates next to PHS in energy storage technologies. CAES require more space and large installation time. Battery storage systems such as li-ion, zinc bromide and flow batteries require less space and require minimum time for installations [9]. The battery storage can offer more than 90% round trip efficiency. 450 MW sodium sulphur storage system in Japan and 54 MW Lithium-ion battery storage system in South Korea are examples for recent grid level installations [10]. Most of the utilities in European Union as well as in United States have adopted policies to acquire energy storage at least to a level of 1% their peak capacity by the end of 2020 [11]. A hybrid energy storage system utilising super conducting magnetic energy storage and battery [12], co-utilisation of battery and thermal units in wind farms [13] are other examples of optimum integrated operation using energy storage. Apart from the advantages obtained by the installation of storage, the technology need to be analysed based upon energy return from the investments made [14]. With the introduction of modular grid level storage systems, which require only few months for the installations and minimum space, the cost for the storage has come down [15].

In this paper, advantages of using battery energy storage for grid level support of a wind electric generator (WEG) are investigated by the use of artificial neural networks (ANN) controller and its DSP implementation. A battery storage supported WEG along with controllers is modelled. ANN controller which is having inherent learning capability is developed to regulate the power flow between wind generator and utility grid based upon the state of charge (SOC) of battery. The proposed algorithm and the corresponding controller are implemented in MATLAB/Simulink as well as in the DSP processor. The real time data exchange between Simulink and the target floating point DSP processor TMSF32028335 is realised. The controller implementation in Simulink and the DSP processor shows the generality of the proposed control strategy for real time operation. The system with BESS is compared with one without energy storage.

2 Wind electric system model

To illustrate the highly varying nature of wind speed, the raw wind data from a one of the wind farm located at Theni district of south India is collected and presented in the Fig. 1. The 10 min average wind speed presented for the year of 2011 shows that site is having high turbulent wind with an annual average speed of 6.71 m/s. By fitting the well-known Weibull distribution to the wind data the

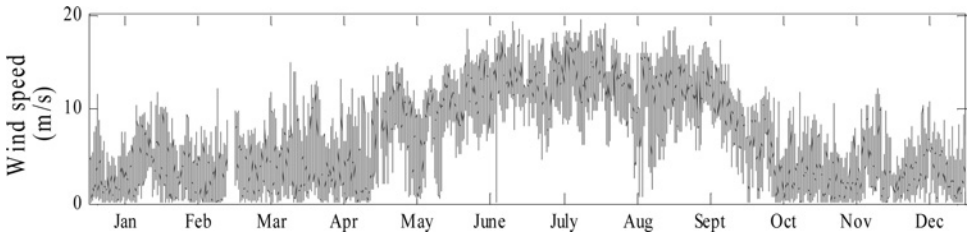

Fig. 1 *Wind speed representation of wind farm Theni for the year 2011*

scale and shape parameter are calculated to be 7.52 m/s and 1.35, respectively.

The WEG system considered for the analysis in this paper is shown in the Fig. 2. The system consists of pitch controlled variable speed wind turbine and back to back converter with DC-link connected to utility grid. Battery storage is added to WEG system at the point of common coupling (PCC).

2.1 Wind turbine model

The power available in the wind is proportional to the cube of wind speed and the power extracted by wind turbine is related to the power coefficient, which in turn is a function of the tip speed ratio and pitch angle of turbine blade. The detailed modelling of wind turbine can be found in [16].

In direct driven technology, gear box is avoided which is one of the advantages of the system [17]. Hence the overall mass of the system and time constants associated with the mathematical models get reduced. The usual range of inertia time constants in per unit for direct driven PMSG based systems is 3 to 8 s. For the 2.5 MW system considered, the inertia time constant is calculated as 5.3 s.

2.2 Modelling of permanent magnet synchronous generator

The model of a synchronous generator presented by Kundur [18] is modified to be used for permanent magnet synchronous generator (PMSG) eliminating the rotor excitation and including the permanent magnet characteristics. Stator winding of PMSG is considered to have equal turns per phase along both the axes. Rotor flux is assumed to be concentrated along d axis and no flux along q axis. Sinusoidal excitation is considered for PMSG and the need for a step up converter between two back to back converters is eliminated. Rotor flux is assumed to be constant.

The d and q model of PMSG can be represented using (1)–(3)

$$\frac{d}{dt}i_{ds} = \frac{\omega_e}{x_d}\left(-u_{ds} - r_s \cdot i_{ds} + \frac{\omega}{\omega_e}x_q \ldots i_{qs}\right) \tag{1}$$

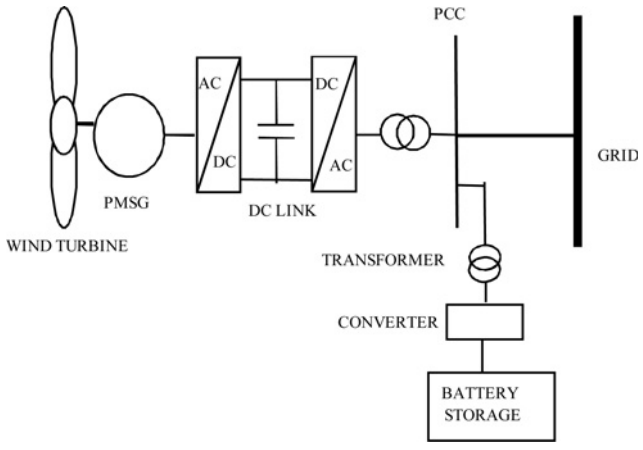

Fig. 2 *Variable speed WEG system with battery storage*

$$\frac{d}{dt}i_{qs} = \frac{\omega_e}{x_q}\left(-u_{qs} - r_s \cdot i_{ds} - \frac{\omega}{\omega_e}(x_d i_{ds} + \psi_m)\right) \tag{2}$$

$$T_e = \psi_d \cdot i_{qs} - \psi_q \cdot i_{ds} \tag{3}$$

where

$$\psi_q = x_q i_{qs} \tag{4}$$

$$\psi_d = x_d \cdot i_{ds} + \psi_m \tag{5}$$

where, i_{ds}, i_{qs} are d and q axis generator current, u_{ds}, u_{qs} are terminal voltage, x_q, x_d are stator reactance, ψ_d, ψ_q are flux linkage along the direct axis and quadrature axis, r_s is stator resistance, ψ_m represents flux linkage provided by permanent magnets and ω_e is basic electrical speed of the generator. Moreover $\omega_e = \omega \times p/2$ where p is the number of poles. The per unit generator terminal voltage, $V_s = \sqrt{u_{ds}^2 + u_{qs}^2}$. The parameters of the 2.5 MW WEG used in the simulation study are given in Tables 1 and 2.

2.3 Modelling of controlled rectifier, DC-link and inverter

Using the fast average $d-q$ model of the converter, the terminal voltage of PMSG, the direct and quadrature axis voltages u_{qs} and u_{ds} can be expressed in terms of the DC-link voltage, modulation ratio m_1 and control angle α_1 using (6) and (7)

$$u_{qs} = m_1 V_{dc}\cos(\alpha_1) \tag{6}$$

$$u_{ds} = -m_1 V_{dc}\sin(\alpha_1) \tag{7}$$

The modulation index m_1 of the generator side converter is controlled by PI controller taking the set value of desired terminal voltage V_s of PMSG and actual value. The control angle α_1 is found by a controller by considering the desired speed of the drive train according to the wind speed and actual speed. The grid side converter output voltages and currents are indicated using u_{dc}, u_{qc}, i_{qc} and i_{dc}. The modulation ratio m_2 of the grid side converter is controlled by a controller taking the set value of reactive power exchange with the grid and actual value. The control angle α_2 is deduced using a PI controller comparing the set value of DC-link voltage and actual value. The grid side converter output voltages

Table 1 Wind turbine parameters

Description	Parameter
rated power	2.5 MW
no. of blades	3
control	Pitch control
blade diameter	40 m
air density	1.1 Kg/m^3
inertia constant	5.8 pu
cut in wind speed	3 m/s
cut off wind speed	25 m/s
rated wind speed	14 m/s

IET Gener. Transm. Distrib., 2015, Vol. 9, Iss. 10, pp. 937–946

Table 2 PMSG parameters

Description	Parameter
rated MVA	2.5
no. of pole pairs	34
x_d, x_q	0.5 pu
r_d, r_q	0.02pu
ψ_m	0.89 pu

can be expressed in terms of m_2, α_2 and V_{dc} using (8) and (9)

$$u_{qc} = m_2 V_{dc} \cos(\alpha_2) \tag{8}$$

$$u_{dc} = -m_2 V_{dc} \sin(\alpha_2) \tag{9}$$

The MATLAB implementation of the controllers for controlled rectifier and inverter are shown in Fig. 3 and PI controller parameters are provided in Table 3.

DC-link voltage can be represented [19] in terms of the current flowing into and out of it (10)–(12)

$$\frac{d}{dt} V_{dc} = \frac{1}{C}(i_v - i_d) \tag{10}$$

where, C is DC-link capacitance, V_{dc} is DC-link voltage, i_d and i_v are current flowing out of the grid side converter and current coming from the generator side converter

$$i_v = \frac{1}{v_{dc}}(u_{ds} i_{ds} + u_{qs} i_{qs} - p_{vloss}) \tag{11}$$

$$i_d = \frac{1}{v_{dc}}(u_{dc} i_{dc} + u_{qc} i_{qc} - p_{dloss}) \tag{12}$$

where, p_{vloss} and p_{dloss} account for the converter losses.

Decoupling between generator and utility grid is provided by a constant DC-link voltage. When this is made possible smooth exchange of active and reactive power to the grid can be achieved.

2.4 Transmission line and grid model

The dq model of the transmission line can be represented using the (13) and (14)

$$\frac{x_{tl}}{\omega_o}\frac{d}{dt} i_{dtl} = v_{d1} - v_{d2} - R_{tl} i_{dtl} - \omega_o x_{tl} i_{qtl} \tag{13}$$

Table 3 Proportional integral gains for PI controllers

Controller	K_p	K_i
PI_{11}	1.31	11
PI_{12}	6	83
PI_{21}	1.3	62
PI_{22}	5.6	54
PI_{31}	0.11	11.3
PI_{32}	2.17	33
PI_{33}	5.3	121

$$\frac{x_{tl}}{\omega_o}\frac{d}{dt} i_{qtl} = v_{q1} - v_{q2} - R_{tl} i_{qtl} + \omega_o x_{tl} i_{dtl} \tag{14}$$

where, i_{dtl}, i_{qtl} are transmission line currents, V_{d1}, V_{d2}, V_{q1}, V_{q2} are direct and quadrature axis voltages at both ends of the transmission line, R_{tl}, x_{tl} are transmission line resistance and inductance, ω_o is average synchronous frequency in the network. The model of the transmission line is given in Fig. 4.

For the analysis, the grid is considered as a stiff system. Accordingly grid voltage is taken as 1 pu and δ is assumed to be zero [20].

2.5 Battery energy storage system (BESS) model and control strategy

To reduce the stress at the PCC and to make sure that scheduled energy is dispatched to the grid, battery storage is added at the PCC [21]. The optimum position of the storage system will determine how far it could support the grid [1]. The dynamic equation used to represent BESS is given in (15)

$$\frac{d}{dt}\begin{bmatrix} i_{dbes} \\ i_{qbes} \\ V_{dcbes} \end{bmatrix} = \begin{bmatrix} \frac{-R_{bes}}{x_{bes}} & \frac{w}{w_e} & 0 \\ \frac{w}{w_e} & \frac{-R_{bes}}{x_{bes}} & 0 \\ \frac{s_1}{C_{bes}} & \frac{s_2}{C_{bes}} & \frac{-R_b R_{dc}}{C(R_b + R_{dc})} \end{bmatrix} \begin{bmatrix} i_{dbes} \\ i_{qbes} \\ V_{dcbes} \end{bmatrix} + w_e \begin{bmatrix} \frac{V_{dcpcc}}{x_{bes}} \\ \frac{V_{qcpcc}}{x_{bes}} \\ \frac{V_{bbat}}{R_b C_{bess}} \end{bmatrix} + \frac{w_e}{x_{bes}} \begin{bmatrix} V_{dcbes} S_1 \\ V_{dcbes} S_2 \\ 0 \end{bmatrix} \tag{15}$$

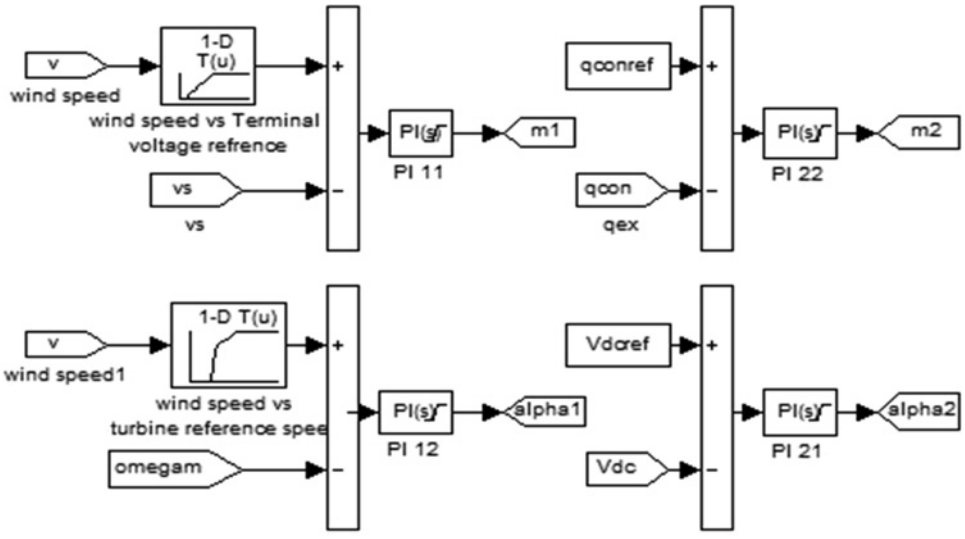

Fig. 3 *Controller implementation of controlled rectifier and inverter*

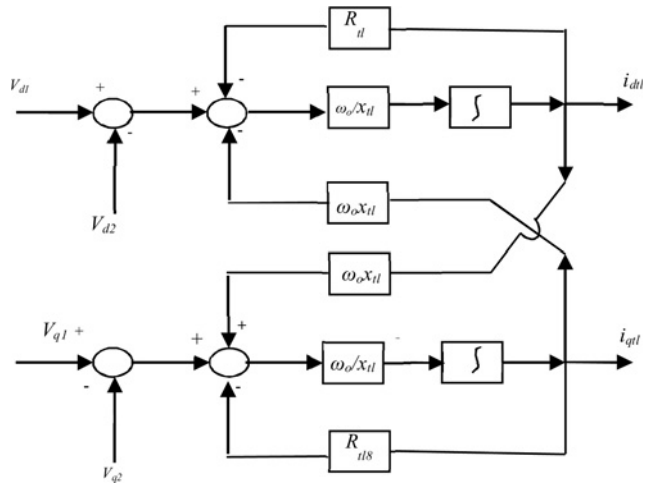

Fig. 4 *Transmission line model*

where $S_1 = m_3\sin(\alpha_3)$, $S_2 = m_3\cos(\alpha_3)$, m_3, α_3 are modulation index and converter angle for BESS inverter, $i_{d\text{bes}}$, $i_{q\text{bes}}$ are BESS currents, V_{dcbes} is voltage across DC capacitor, R_{bes}, x_{bes} represents BESS transformer resistance and reactance, V_{bbat} is battery voltage, R_{b} represents self-discharging loss of battery, R_{dc} represents charging and discharging loss of battery and C_{bes} is battery capacitance.

To ensure optimum scheduling, it is very important to have accurate wind forecasting and the knowledge of SOC of the battery. SOC gives the information regarding how much energy remains in the battery and it is dependent up on internal parameters, temperature and age of the battery. The precise measurement of SOC is still a matter of research. Out of the different methods to measure SOC [4, 22–25], calculation based upon ampere hour counting [25], is used in this paper. SOC at any time t, can be obtained using (16) where Q represents the battery capacity, SOC(0) is the initial SOC, $I(t)$ is the charging or discharging current of the battery

$$\text{SOC}(t) = \text{SOC}(0) - \frac{1}{\text{Q}}\int_0^t I(t)\text{d}t \tag{16}$$

It is very essential to maintain SOC of the battery within the minimum and maximum levels so that the BESS is completely utilised for power scheduling. The preferred levels of battery operation considered are 20–90% of SOC.

To realise the scheduled energy demand, power injected by WEG system to the grid (i_{pWEG} – active current) is compared with the scheduled power (I_{shref}) and the error generated (i_{pref}) is given as the reference power for the BESS. Once the wind power generation is less than the scheduled value, BESS provides the remaining power and when there is excess power than the grid demand, power is absorbed by the BESS. In the BESS controller, the reactive current reference is generated comparing the reference PCC voltage (V_{pccref}) with the actual value (V_{pcc}). From the intermediate control variables e_{R} rand e_{P} the controller will generate the parameters m_3 and α_3 imposing reference power flow from the battery and ensure scheduled power is injected at PCC from wind battery system. The controller configuration for the BESS is shown in Fig. 5. The parameters of the PI controllers of BESS are provided in Table 3. For the scheduled energy dispatch from wind farms, BESS with high MWh rating is required. For the analysis in this paper, a BESS which can support the WEG system up to 50% of its rated capacity for duration of 1 h is considered. Accordingly the energy required to be stored in BESS is calculated as 1.25 MWh.

Table 4 ANN parameters

Description	Parameter
ANN structure	feed forward
no. hidden layers	1
no. hidden layer neurons	5
hidden layer	
activation function	tansigmoid
output activation function	pureline
training method	back propagation
training function	levenberg-marquardt
performance function	mean square error

3 ANN-based controller

Conventional controllers do not exhibit the intelligence to adapt with the varying operating conditions. ANNs have the inherent learning capability and they exhibit excellent set point tracking. A feed-forward ANN consists of N layers of neurons, the dot product

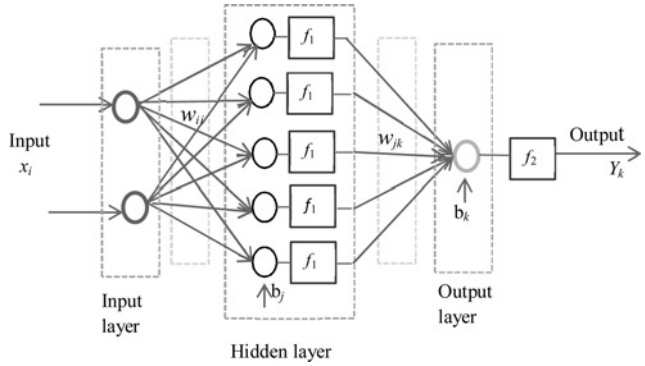

Fig. 6 *Three layer feed forward network*

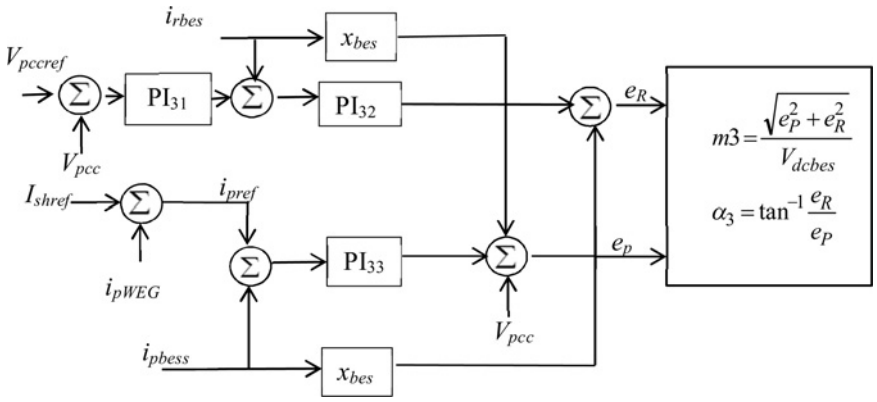

Fig. 5 *BESS controller*

IET Gener. Transm. Distrib., 2015, Vol. 9, Iss. 10, pp. 937–946

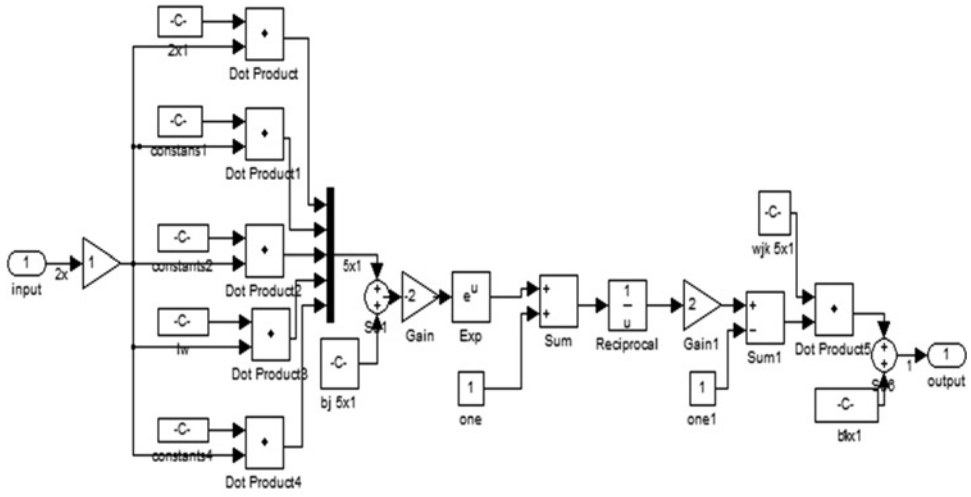

Fig. 7 *MATLAB implementation of a three layer feed-forward ANN*

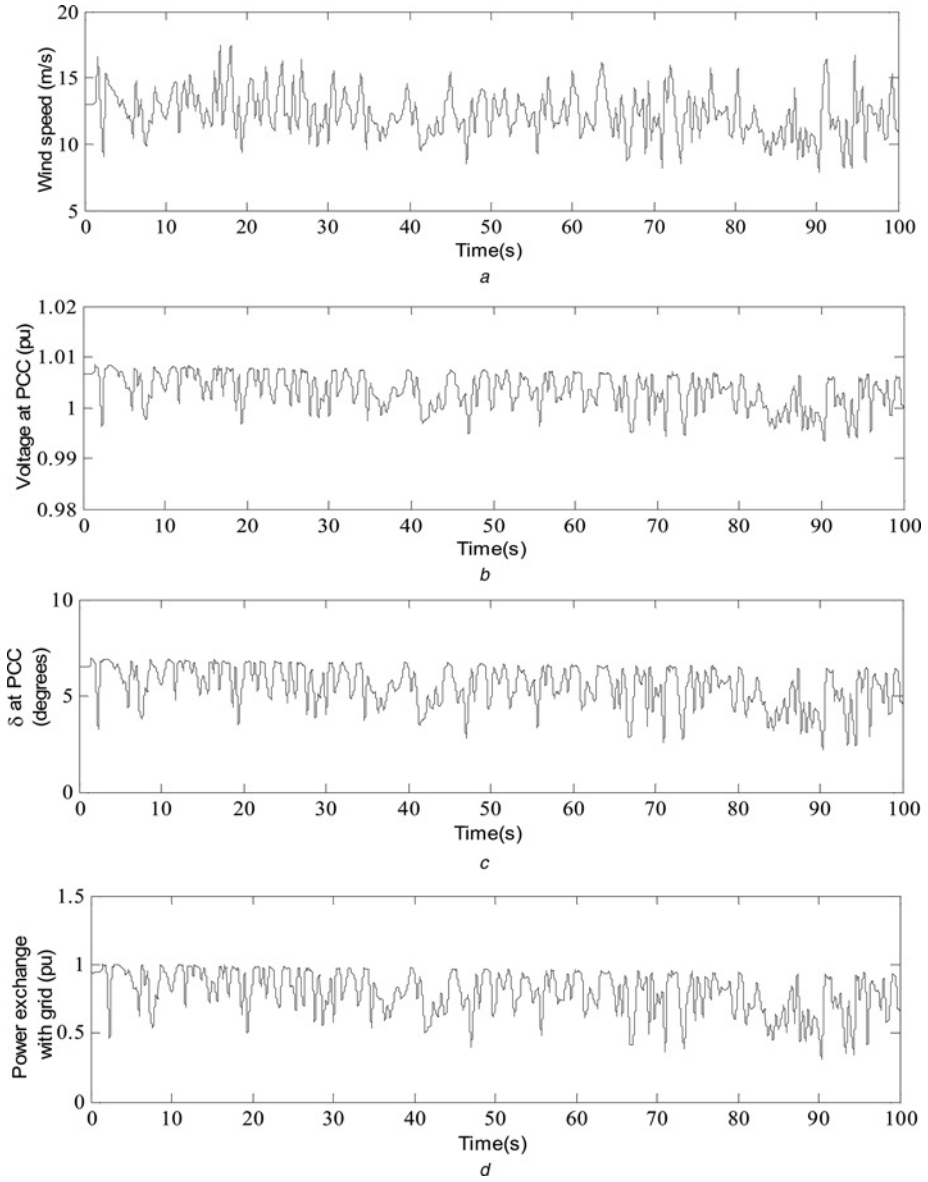

Fig. 8 *Response of simulated WEG system without energy storage in*

a Wind speed
b Voltage at PCC
c Power angle (δ) at PCC
d Power exchange with grid

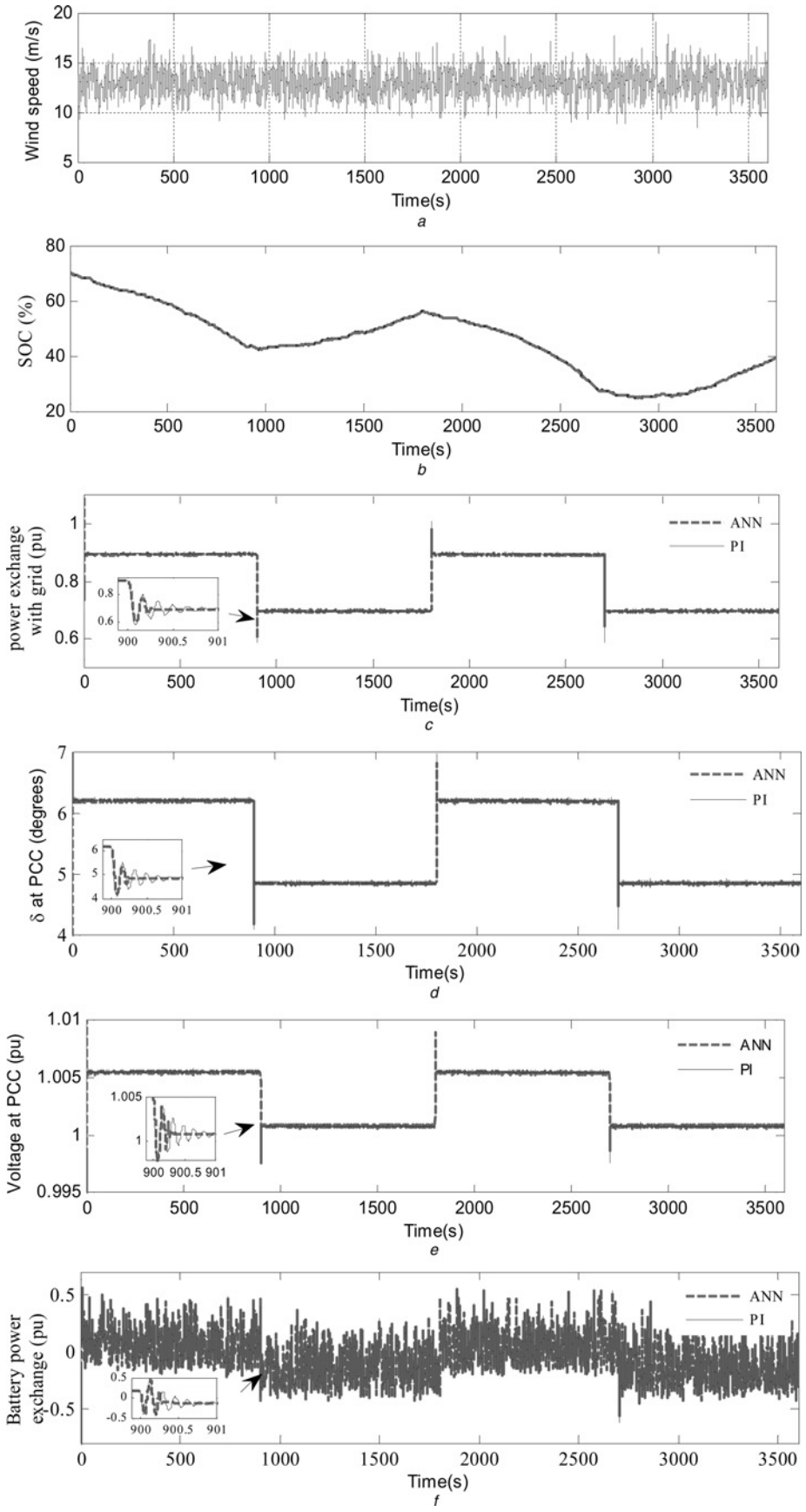

Fig. 9 *Comparison of response of WEG system to the wind speed variation with energy storage during simulation using PI and ANN controller in*

a Wind speed
b SOC of battery
c Power exchange with grid
d Power angle (δ) at PCC
e Voltage at PCC
f Battery power exchange

IET Gener. Transm. Distrib., 2015, Vol. 9, Iss. 10, pp. 937–946

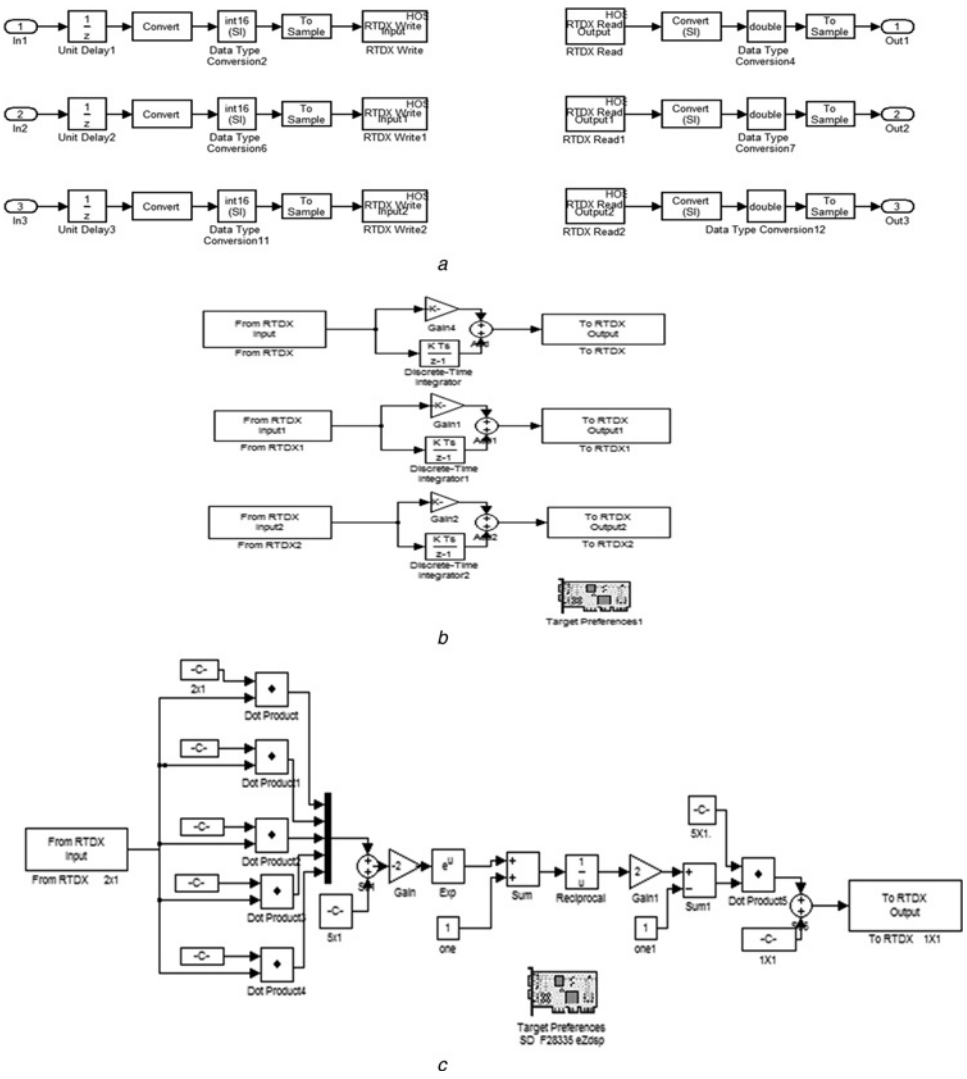

Fig. 10 *DSP implementation of PI and neural network controllers*

a Use of From RTDX and To RTDX blocks to define communication channels in Simulink
b Target implementation of PI controllers
c Target implementation of neural network controllers

weight functions, net input functions and specified transfer functions. Each neuron of the different network layers are connected to previous layer and next layer neurons through proper weights. All layers have biases and the last layer is the network output. Considering the robust nature of neural network, to implement the proposed control algorithm, a three layer feed-forward back propagation network is modelled with parameters as given in Table 4. The feed forward neural network model used in this analysis is as given in Fig. 6.

The output of a three layer feed forward network can be calculated using the (17) and (18) where the network consists of i inputs, k outputs and j hidden layer neurons. V_j represents the output from the jth neuron in the hidden layer. w_{ij} *is* the input weight between the ith neuron of input layer and the jth neuron of hidden layer, b_j represents the bias to the jth hidden layer neuron and f_1 represents the hidden layer activation function. Y_k represents the kth output, w_{jk} represents the weight between the jth neuron of hidden layer and the kth neuron of output layer, b_k the output layer bias and f_2 represents the output layer activation function

$$V_j = f_1\left(\sum (x_i \cdot w_{ij}) + b_j\right) \tag{17}$$

$$Y_k = f_2\left(\sum (V_j \cdot w_{jk}) + b_k\right) \tag{18}$$

The training of the neural network is the most crucial part of formation of a good neural network. Here in this work, the network is trained based up on back propagation algorithm and done off line. In the back propagation algorithm, initially, first set of input data are fed to the network resulting in a particular output. The obtained output is compared with the corresponding target in the training set and error is calculated. Based on the error obtained the layer weights as well as the bias values at each layer are updated. The error calculation, and the weight updating process continues till the error obtained is well within the specified limit and measurable error is negligible. The updating of weights starts from the output layer in each iteration. The new weights w_{ij} for each layer is calculated based on the (19) and (20). Where w'_{ij} is the previous weight, lr learning rate, e_k the error term calculated during the iteration and t_k the target

$$w_{ij} = w'_{ij} + lr \cdot e_k \cdot x_i \tag{19}$$

$$e_k = Y_k \cdot (1 - Y_k) \cdot (t_k - Y_k) \tag{20}$$

The error term e_k used for the back propagation is the dot product of output Y_k, the complement of Y_k and the actual difference between output t_k and corresponding target Y_k. The MATLAB implementation of each ANN-based controller is shown in

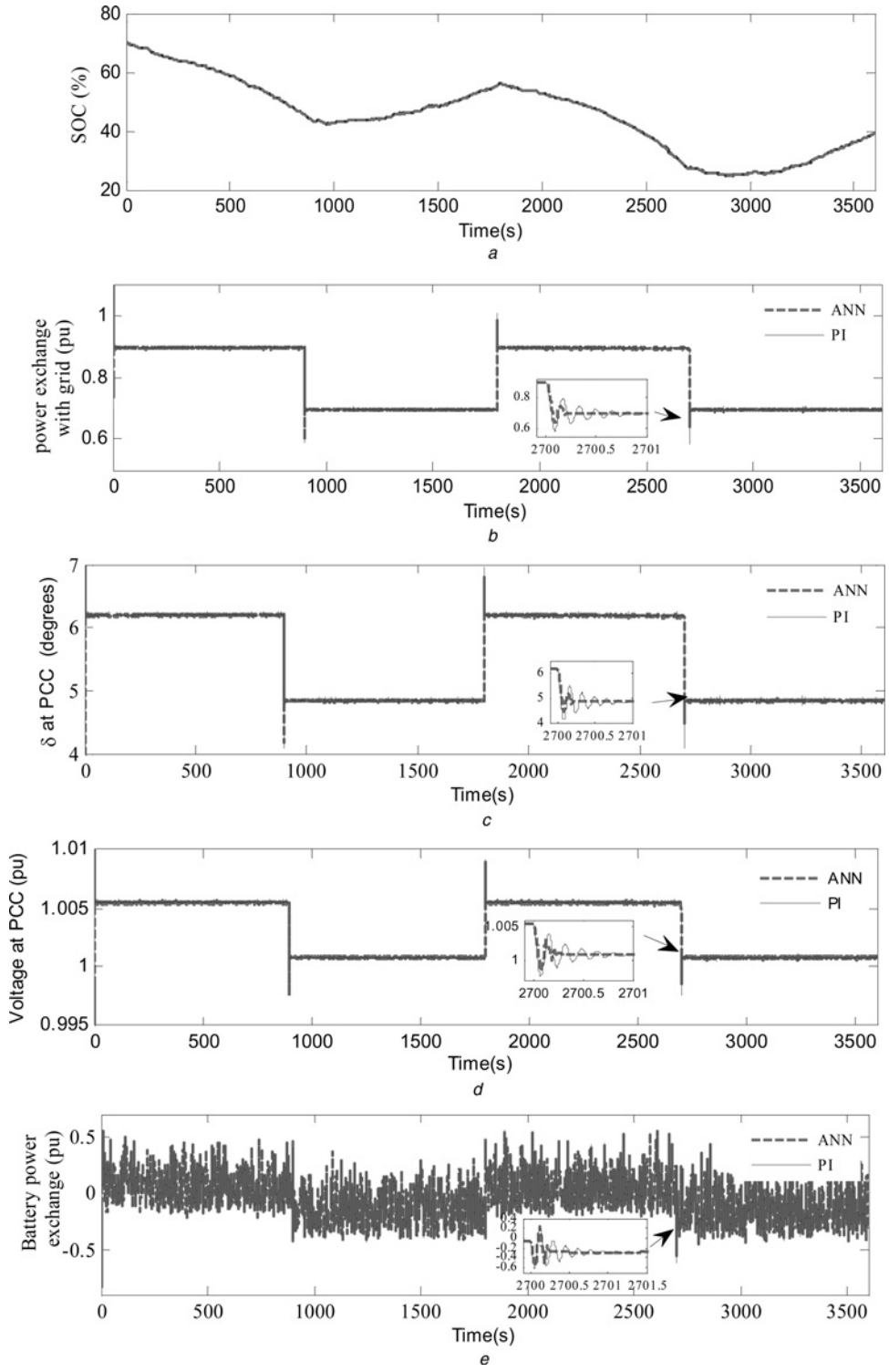

Fig. 11 *Performance comparison of controllers implemented in DSP in*

a SOC of the battery
b Power exchange with grid
c Power angle (δ) at PCC
d Voltage at PCC
e Battery power exchange

Fig. 7. The training of the ANN controller is done off line collecting data from the system while using PI controller for a duration of 100 s (10 000 samples). Testing and verification of the developed controller is done replacing all the PI controllers of the BESS system with ANN controllers and performance is analysed in simulation and in real time implementation in DSP.

4 MATLAB/Simulink simulation

4.1 WEG system without energy storage

To visualise the stress offered by the varying wind speed on the grid, the WEG system is simulated without the support of energy storage.

IET Gener. Transm. Distrib., 2015, Vol. 9, Iss. 10, pp. 937–946

The varying wind speed selected for the simulation work in the paper is shown in the Fig. 8*a*. The system parameters considered for the performance evaluation are the voltage at PCC as shown in the Fig. 8*b*, the power angle delta (δ) at PCC in Fig. 8*c* and the power exchange with grid in Fig. 8*d*. It can be observed that along with the variation of the wind speeds, the power injected by the WEG system to the grid changes as shown in the Fig. 8*d*. The power injected is limited to 1 pu by the pitch angle controller for wind speed above the rated speed of 14 m/s. During the time when wind speed is below the rated value, corresponding variation can be found in the power angle (δ), voltage at PCC and power exchange with grid. Owing to these sudden parameter changes corresponding to high turbulent wind speed at PCC, the grid will always be at a stressed state. The stress occurring at the PCC can turn in to a state of system instability on the event of any contingency either at generation side or at the grid side. The situation can be improved to greater extent by the use of energy storage.

4.2 Comparison of performance of WEG system with energy storage using PI and ANN controller

To facilitate reduced stress at PCC and to ensure desired/scheduled power flow to the grid, a battery storage system is incorporated at the PCC. The simulation is carried out using the conventional PI controller as well as the ANN-based controller. Simulation duration of one hour is divided into four slots of 15 min each. The wind speed considered for the study is given in Fig. 9*a*. Scheduling of power dispatch has to be made with the help of wind prediction and calculating SOC of the battery. Initial SOC of the BESS is assumed to be at 70%. Depending upon the predicted wind speed and the SOC of battery, power schedule is fixed at 0.9 pu. At the end of first time slot, SOC reaches to 42% as in Fig. 9*b*. To ensure that SOC does not reach the minimal level of 20% in the immediate time slot, power schedule is changed to 0.7 pu. As the SOC has improved at the end of second time slot to 58%, power schedule is raised to 0.9 pu in the third time slot. At 2700s, scheduled power is further reduced to 0.7 pu and SOC is raised to a value of 39% at the end of fourth time slot. It is observed that with the ANN controller, set point changes in power schedule are tracked at a faster rate than with the PI controller as presented in Fig. 9*c*. The scheduled energy set point changes are reflected in the power angle (δ) and voltage at PCC as shown in Figs. 9*d* and *e*. Fig. 9*f* shows the power exchange by BESS. A positive value in the battery power indicates the power supplied by the battery (discharge) and the negative value indicates the power consumed (charging) by the battery. The mean square error while using PI controllers are 0.44% whereas using ANN is 0.40%. During the time when scheduled power references are changed the system parameters settle to the new value in 1 s when using PI controllers whereas it takes only 0.2 s to settle to a new value when ANN controller are used. The reduced time for settling of the power angle and voltage at PCC while using ANN controller shows the inherent learning capability and excellent tracking ability of the ANN network. It can also be understood that when there is BESS support for the WEG system the wind speed changes are not reflected at the PCC and the system is more stable.

5 DSP implementation

The conventional PI controllers as well as the ANN controller are realised and implemented in digital signal processor. For the real time implementation the target selected is Texas instruments TMS320F28335 eZdsp processor. This is a floating-point Digital Signal Controller. The integrated on board JTAG emulation incorporated in the spectrum digital starter kit and USB interface to the host PC, enable real time communication between the target and the host. Integrated Development Environment Code Composer Studio™ serves as the software interface between MATLAB /Simulink and the target processor [26]. Simulink model interacts with the target application in real-time. The read-from and write-to RTDX Simulink blocks used in the simulation define communication channels between Simulink and the target. Fig. 10*a* shows how these blocks are used in the model to make Simulink interact with the DSP processor. The DSP implementation of PI and neural network controllers are presented Figs. 10*b* and *c*. The synchronous communication between the Simulink and DSP processor is enabled throughout the process running time. The conventional PI controllers as well as the ANN controllers are implemented in the target processor.

The wind speed variation as well as the set point changes used for simulation is considered for DSP implementation of controllers. The system parameters considered during analysis are presented in Fig. 11. It is found that the performances of the system during simulation and while using DSP processor are similar. The similarity observed during simulation and DSP implementation validates the control algorithm.

6 Conclusion

The excess generation of electricity during the time of low demand and inadequate generation during peak hours are always a bottle neck in the renewable integrated grid system. This limitation is overcome to a great extent by the use of storage technologies along with renewables. By suitably charging and discharging the battery, with the help of accurate prediction of wind and measurement of SOC, the problems associated with the intermittent nature of renewable sources can be reduced. The application of battery energy storage for grid level support of WEG is investigated through the use of conventional PI controller and ANN-based controller. The inherent learning nature and the ability of ANN to adapt with the varying operating conditions are demonstrated in this paper. The effective use of the storage system in reducing the stress at the PCC as well as maintaining the scheduled energy dispatch is explained by comparing a WEG system with and without energy storage. The validation of the control algorithm is done using Simulink simulation and its DSP implementation. Real time data exchange between the MATLAB/SIMULINK and DSP processor is achieved. The analogous results obtained during simulations as well as in the target implementation shows the suitability of the proposed control strategy for real time operation.

7 Acknowledgement

The authors gratefully acknowledge the support offered by the Government of India, Ministry of defence, Defence Research and Development Organization of India (DRDO) under the grant no. ERIP/ER/1006010/M/01/1268 for this work.

8 References

1 Muñoz, C., Sauma, E., Contreras, J., Aguado, J., de la Torre, S.: 'Impact of high wind power penetration on transmission network expansion planning', *IET. Gener. Transm. Distrib.*, 2012, **6**, (12), pp. 1281–1291
2 Vazquez, S., Lukic, S.M., Galvan, E., Franquelo, L.G., Carrasco, J.M.: 'Energy storage systems for transport and grid applications', *IEEE Trans. Ind. Electron.*, 2010, **57**, (12), pp. 3881–3895
3 Barnhart, C.J., Dale, M., Brandt, A.R., Benson, S.M.: 'The energetic implications of curtailing versus storing solar- and wind-generated electricity', *Energy Environ. Sci.*, 2013, **6**, (10), pp. 2804–2810
4 Xu, Y., Singh, C.: 'Power system reliability impact of energy storage integration with intelligent operation strategy', *IEEE Trans. Smart Grid*, 2014, **5**, (2), pp. 1129–1137
5 Zhang, G., Wan, X.: 'A wind-hydrogen energy storage system model for massive wind energy curtailment', *Int. J. Hydrog. Energy*, 2014, **39**, (3), pp. 1243–1252
6 Li, X., Hui, D., Lai, X.: 'Battery energy storage station (BESS)-based smoothing control of photovoltaic (PV) and wind power generation fluctuations', *IEEE Trans. Sustain. Energy*, 2013, **4**, (2), pp. 464–473
7 Du, W., Wang, H.F., Cao, J., Xiao, L.Y.: 'Robustness of an energy storage system-based stabiliser to suppress inter-area oscillations in a multi-machine power system', *IET. Gener. Transm. Distrib.*, 2012, **6**, (4), pp. 339–351

8 Weisser, D., Garcia, R.S.: 'Instantaneous wind energy penetration in isolated electricity grids: concepts and review', *Renew. Energy*, 2005, **30**, (8), pp. 1299–1308
9 Sebastian, R.: 'Modelling and simulation of a high penetration wind diesel system with battery energy storage', *Int. J. Electr. Power Energy Syst.*, 2011, **33**, (3), pp. 767–774
10 Tarnowski, G.C., Philip, C.K.: 'Frequency control in power systems with high wind Power Penetration'. Ninth Int. Workshop on Large-scale Integration of Wind Power and Transmission Networks for Offshore Wind Farms, Québec, Canada, October 2010
11 Technical report: 'Grid energy storage' (U.S. Department of Energy, 2013)
12 Shim, J.W., Cho, Y., Kim, S.-J., Min, S.W., Hur, K.: 'Synergistic control of SMES and battery energy storage for enabling dispatchability of renewable energy sources', *IEEE Trans. Appl. Supercond.*, 2013, **23**, (3), pp. 5701205–5701209
13 Lee, T.Y.: 'Optimal wind-battery coordination in a power system using evolutionary iteration particle swarm optimisation', *IET. Gener. Transm. Distrib*, 2008, **2**, (2), pp. 291–300
14 Hasani-Marzooni, M., Hosseini, S.H.: 'Trading strategies for wind capacity investment in a dynamic model of combined tradable green certificate and electricity markets', *IET. Gener. Transm. Distrib*, 2012, **6**, (4), pp. 320–330
15 Denholm, P., Jorgenson, J., Hummon, M., *et al*.: 'The Value of Energy Storage for Grid Applications'. National Renewable Energy Laboratory Technical Report, NREL/TP-6A20-58465, May 2013
16 Hier, S.: 'Grid integration of wind energy conversion systems' (John Wiley and Sons, 1998)
17 Kurian, S., Sindhu, T.K., Cheriyan, E.P.: 'Review on developments in wind energy generation and its integration to utility grid', *Int. Rev. Model. Simul.*, 2013, **6**, (5), pp. 1523–1532
18 Kundur, P.: 'Power system stability and control' (McGraw-Hill, 1994)
19 Krause, P.C., Wasynczuk, O., Sudhoff, S.D.: 'Analysis of electric machinery and drive systems' (Wiley-IEEE Press, 2002, 2nd edn.)
20 Padiyar, K.R.: 'Facts controllers in power transmission and distribution' (New age international (P) Ltd, 2007)
21 EL-Shimy, M.: 'Optimal site matching of wind turbine generator: case study of the Gulf of Suez region in Egypt', *Renew. Energy*, 2010, **35**, (18), pp. 1870–1878
22 Riffonneau, Y., Bacha, S., Barruel, F., Ploix, S.: 'Optimal power flow management for grid connected PV systems with batteries', *IEEE Trans. Sustain. Energy*, 2011, **2**, (3), pp. 309–320
23 Chiasson, J., Vairamohan, B.: 'Estimating the state of charge of a battery', *IEEE Trans. Control Syst. Technol.*, 2005, **13**, (3), pp. 465–470
24 Xing, Y., He, W., Pecht, M., Tsui, K.L.: 'State of charge estimation of lithium-ion batteries using the open-circuit voltage at various ambient temperatures', *Appl. Energy*, 2014, **113**, pp. 106–115
25 Xiao, B., Shi, Y., He, L.: 'A universal state-of-charge algorithm for batteries'. 47th ACM/IEEE Design Automation Conf. (DAC), Canada, 2010
26 MATLAB EMBEDDED IDE LINK 4 – for use with Texas Instruments Code Composer Studio User's Manual. www.Mathworks.com